Performance Analysis of a 3-2-1 Pose Estimation Device

Federico Thomas, Erika Ottaviano, Lluís Ros, Marco Ceccarelli

Abstract— **This paper deals with the problem of estimating the pose of a rigid moving object by measuring the length of six wires attached to it. Since wires can be seen as extensible legs, this problem is equivalent to that of solving the forward kinematics of a six-degree-of-freedom parallel manipulator. Among all possible locations for the attachments on the moving object, the "3-2-1" configuration is shown to exhibit a high number of favorable properties. The performance analysis of this particular configuration is addressed by finding analytic expressions for the estimated pose covariance matrix and the expected value of the pose estimation error, or bias error, which has been omitted in the previous analysis of wire-based tracking devices. This analysis takes advantage of a formulation for trilateration based on Cayley-Menger determinants which is mathematically more tractable compared to previous ones because all involved terms are determinants with geometric meaning. This accommodates a more thorough investigation of the properties of the device.**

Keywords— **Pose estimation devices, parallel manipulators, kinematic singularities, Cayley-Menger determinants, bias error.**

I. Introduction

Many systems for measuring the pose, i.e. position and orientation, of moving objects, also known as tracking systems, have been developed. They can be classified according to the measuring principle and used technology. Most of these systems are based on cameras, theodolites, laser and wires which are able to provide distance measurements by triangulation or trilateration techniques. Trilateration and triangulation determine the relative position between points by using the geometry of triangles or tetrahedra. Triangulation uses measurements of both distances and angles, whereas trilateration uses only distance measurements.

Tracking systems can also be classified according to their characteristics, such as accuracy, resolution, cost, measurement range, portability, and calibration requirements. Laser tracking systems exhibit good accuracy, which can be less than $1\mu m$ if the system is well calibrated. Unfortunately, they are very expensive, their calibration procedure is time consuming, and they are sensitive to the environment. Vision systems have an accuracy of $0.1mm$, they are low cost portable devices but their calibration procedure can be complicate. Wire-based systems can reach an accuracy of $0.1mm$, they are also low cost portable devices but capable of measuring large displacements. Moreover, they exhibit a good compromise among accuracy, measurement range, cost and operability.

F. Thomas and L. Ros are with the Institut de Robòtica i Informàtica Industrial (CSIC-UPC), Llorens Artigas 4-6, 2 planta, 08028 Barcelona, Spain (e-mails: {fthomas, llros}@iri.upc.es).

E. Ottaviano and M. Ceccarelli are with the Laboratorio di Robotica e Meccatronica Università degli Studi di Cassino, Via G. Di Biasio, 43, 03043 Cassino, Italy (e-mails: {ottaviano, ceccarelli}@unicas.it).

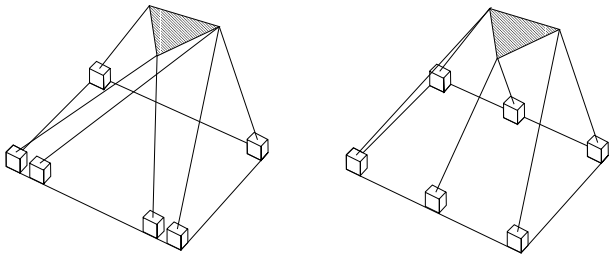

Fig. 1. The "3-2-1" **(a)** and "2-2-2" **(b)** configurations for wire-based tracking devices as proposed in [9] and [12], respectively.

Wire-based tracking devices consist of a fixed base and a platform connected by six wires whose tension is maintained, while the platform is moved, by pulleys and spiral springs on the base, where a set of encoders give the length of the wires. They can be modelled as six-degree-of-freedom parallel manipulators because wires can be seen as extensible legs connecting the platform and the base by means of spherical and universal joints, respectively.

Dimension deviations due to fabrication tolerances, wire length uncertainties, wire slackness, etc., may result in an unacceptable performance of a wire-based tracking device. In general, the effects of all systematic errors can be eliminated by calibration. Some techniques for specific errors have already been proposed in the literature. For example, a method for compensating the cable guide outlet shape of wire encoders is detailed in [9], and a method for compensating the deflections caused by wire self-weights is described in [12]. In this paper, we will only consider wire length errors which cannot be compensated because of their random nature.

Another indirect source of error is the force exerted by the measuring device itself. Indeed, all commercial wire encoders are designed to keep a large string tension. This is necessary to ensure that the inertia of the mechanism does not result in a wire going slack during a rapid motion. If a low wire force is used, it would reduce the maximum speed of the object to be tracked without wires going slack. On the contrary, if a high wire force is used, the trajectory of the object to be tracked could be altered by the measuring device. Hence, a trade-off between accuracy and speed arises.

An important issue in wire-based tracking devices is the number of attachments on the moving object and how many wires are connected to each attachment. On the base side, no two wire outlets can be made coincident be-

cause of physical limitations. This is not the case on the platform where it is advisable to reduce the number of attachments not only to get simpler pose estimation expressions but also to reduce the risk of wire wrapping. If all attachments would collapse into a single point on the platform, wrapping problems can be avoided. Unfortunately, the minimum number of points for pose measurements is three. Moreover, the maximum number of wires attached to a point is also three, otherwise the lengths of the wires will not be independent. This leads to only two possible configurations for the attachments on the moving object. Both have already been reported in the literature of wire-based tracking devices. Namely,

- *The 2-2-2 configuration.* This configuration was first proposed in [12] for a wire-based tracking device (Figure 1b). The authors overlooked the fact that the kinematics of this configuration was already studied, for example, in [10], [17], and [22] where it was shown that its forward kinematics has 16 solutions. In other words, there are up to 16 poses for the moving object compatible with a given set of wire lengths. These configurations can only be obtained by a numerical method. The lack of a closed-form solution limits the analysis of the effects caused by the different forms of error.
- *The 3-2-1 configuration.* This configuration was proposed in [9] (Figure 1a). The authors present it as a new configuration of a Steward platform thus ignoring that the kinematics of this configuration was already studied, for example, in [16] and [11]. Its direct kinematics can be solved in closed-form by using three consecutive trilateration operations yielding 8 solutions.

Both configurations were compared in [9] in terms of their sensitivity to wire length errors concluding that they have similar properties, but there are at least two reasons that make the 3-2-1 configuration preferable: (a) it has a lower number of forward kinematics solutions, which is useful to avoid ambiguities, and (b) these solutions can be obtained by a closed-form formula, which enables us to perform an algebraic error analysis of the device.

As already mentioned, the forward kinematics solutions for the 3-2-1 configuration can be obtained by three consecutive trilateration operations. Although trilateration can be trivially expressed as the problem of finding the intersection of three spheres, different closed-form solutions have been proposed in the areas of computer graphics [8], robotics [2], aeronautics [15], computational geometry [5], and crystallography [14]. We here rely on the formulation presented in [24] whose main advantage is that all involved terms are determinants with geometric interpretation, allowing a deeper insight into its error analysis.

This paper is organized as follows. Section II introduces the concept of Cayley-Menger bideterminant and gives a closed-form solution to the trilateration problem in terms of this kind of determinants. Next, the forward kinematics and the singularities of the 3-2-1 configuration are analyzed in Section III. The sensitivity of this configuration to wire length errors and the effect of bias errors are tackled in Section IV and Section V, respectively. Thanks to our formulation in terms of Cayley-Menger bideterminants, we will see how the bias error analysis have been greatly simplified. Experimental results are presented in Section VI that exemplify the most relevant characteristics of the 3-2-1 configuration analyzed throughout this paper. Finally, we conclude in section VII summarizing the main results and giving prospects for further research.

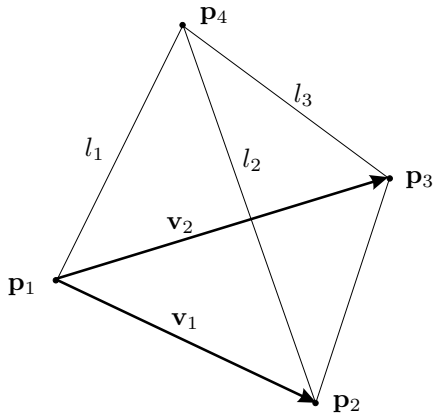

Fig. 2. The trilateration problem consists in, given points $\mathbf{p}_1$, $\mathbf{p}_2$, and $\mathbf{p}_3$, and distances l_1, l_2, and l_3, locating $\mathbf{p}_4$.

II. Cayley-Menger bideterminants and trilateration

The *Cayley-Menger bideterminant* of two sequences of n points, $[\mathbf{p}_1, \ldots, \mathbf{p}_n]$ and $[\mathbf{q}_1, \ldots, \mathbf{q}_n]$, is defined as

$$D(\mathbf{p}_1, \ldots, \mathbf{p}_n; \mathbf{q}_1, \ldots, \mathbf{q}_n) = 2\left(\frac{-1}{2}\right)^n \cdot \left| \begin{array}{ccccc} 0 & 1 & 1 & 1 & 1 \\ 1 & D(\mathbf{p}_1, \mathbf{q}_1) & D(\mathbf{p}_1, \mathbf{q}_2) & \cdots & D(\mathbf{p}_1, \mathbf{q}_n) \\ 1 & D(\mathbf{p}_2, \mathbf{q}_1) & D(\mathbf{p}_2, \mathbf{q}_2) & \cdots & D(\mathbf{p}_2, \mathbf{q}_n) \\ \vdots & \vdots & \vdots & \ddots & \vdots \\ 1 & D(\mathbf{p}_n, \mathbf{q}_1) & D(\mathbf{p}_n, \mathbf{q}_2) & \cdots & D(\mathbf{p}_n, \mathbf{q}_n) \end{array} \right|,$$

where $D(\mathbf{p}_i, \mathbf{q}_j)$ denotes the squared distance between the points $\mathbf{p}_i$ and $\mathbf{q}_j$. This determinant plays a fundamental role in the so-called "Distance Geometry," a term coined by L. Blumenthal in [1] which refers to the analytical study of the Euclidean geometry in terms of invariants without resorting to artificial coordinate systems. Since in many cases of interest the two sequences of points are the same, it will be convenient to abbreviate $D(\mathbf{p}_1, \ldots, \mathbf{p}_n; \mathbf{p}_1, \ldots, \mathbf{p}_n)$ by $D(\mathbf{p}_1, \ldots, \mathbf{p}_n)$, which is simply called a *Cayley-Menger determinant*. This determinant was first used by A. Cayley in 1841 [3], but it was not systematically studied until 1928, when K. Menger showed how it could be used to study convexity and other basic geometric properties [19].

Given three points in space, say $\mathbf{p}_1$, $\mathbf{p}_2$, and $\mathbf{p}_3$, the trilateration problem consists in finding the location of another point, say $\mathbf{p}_4$, whose distance to these three points is known (Figure 2). According to the results presented in [24], $\mathbf{p}_4$ can be expressed as

$$\mathbf{p}_4 = \mathbf{p}_1 + k_1\mathbf{v}_1 + k_2\mathbf{v}_2 \pm k_3(\mathbf{v}_1 \times \mathbf{v}_2), \qquad (1)$$

where $\mathbf{v}_1 = \mathbf{p}_2 - \mathbf{p}_1$, $\mathbf{v}_2 = \mathbf{p}_3 - \mathbf{p}_1$, the $\pm$ sign accounts for the two mirror symmetric solutions to the plane defined by $\mathbf{p}_1$, $\mathbf{p}_2$, and $\mathbf{p}_3$, and

$$k_1 = -\frac{D(\mathbf{p}_1, \mathbf{p}_2, \mathbf{p}_3; \mathbf{p}_1, \mathbf{p}_3, \mathbf{p}_4)}{D(\mathbf{p}_1, \mathbf{p}_2, \mathbf{p}_3)},$$
$$k_2 = \frac{D(\mathbf{p}_1, \mathbf{p}_2, \mathbf{p}_3; \mathbf{p}_1, \mathbf{p}_2, \mathbf{p}_4)}{D(\mathbf{p}_1, \mathbf{p}_2, \mathbf{p}_3)}, \quad (2)$$
$$k_3 = \frac{\sqrt{D(\mathbf{p}_1, \mathbf{p}_2, \mathbf{p}_3, \mathbf{p}_4)}}{D(\mathbf{p}_1, \mathbf{p}_2, \mathbf{p}_3)}.$$

Many other formulations for trilateration are expressed according to a specific coordinate frame. For example, in [9], the XY plane is the plane defined by $\mathbf{p}_1$, $\mathbf{p}_2$ and $\mathbf{p}_3$, the X axis is defined by the line containing $\mathbf{p}_1$ and $\mathbf{p}_2$ and the origin of the frame is located at $\mathbf{p}_1$. The formulation given here is coordinate-free. Nevertheless, the most interesting aspect of the proposed formulation compared to all others is that it is mathematically more tractable because all involved terms are determinants with geometric meaning. Actually,

$$D(\mathbf{p}_1, \mathbf{p}_2, \mathbf{p}_3, \mathbf{p}_4) = 36V^2, \quad (3)$$

where V is the volume of the tetrahedron defined by $\mathbf{p}_1$, $\mathbf{p}_2$, $\mathbf{p}_3$, and $\mathbf{p}_4$. Hence, $D(\mathbf{p}_1, \mathbf{p}_2, \mathbf{p}_3, \mathbf{p}_4) = 0$ if, and only if, $\mathbf{p}_1$, $\mathbf{p}_2$, $\mathbf{p}_3$, and $\mathbf{p}_4$ lie on a plane.

$$D(\mathbf{p}_1, \mathbf{p}_2, \mathbf{p}_3) = 4A^2, \quad (4)$$

where A is the area of the triangle defined by $\mathbf{p}_1$, $\mathbf{p}_2$ and $\mathbf{p}_3$. Hence, $D(\mathbf{p}_1, \mathbf{p}_2, \mathbf{p}_3) = 0$ if, and only if, $\mathbf{p}_1$, $\mathbf{p}_2$, and $\mathbf{p}_3$, are aligned.

$$D(\mathbf{p}_1, \mathbf{p}_2, \mathbf{p}_3; \mathbf{q}_1, \mathbf{q}_2, \mathbf{q}_3) = 2A_1 \cdot 2A_2 \cdot \cos\phi, \quad (5)$$

where A_1 and A_2 are the oriented areas of the triangles $\mathbf{p}_1\mathbf{p}_2\mathbf{p}_3$ and $\mathbf{q}_1\mathbf{q}_2\mathbf{q}_3$, respectively, and ϕ is the dihedral angle between the planes they define.

As a consequence of this geometric interpretation of all terms involved in the formulation, we will be able to accommodate a more thorough investigation of the effects caused by wire length errors, singularities, and bias errors of a 3-2-1 configuration, as shown below.

III. Forward kinematics and singularities

The direct kinematics of the 3-2-1 configuration can be solved by three consecutive trilateration operations. Indeed, according to Figure 3a, given l_1, l_2, and l_3, there are two possible mirror locations for $\mathbf{b}_1$ with respect to the plane defined by $\mathbf{a}_1$, $\mathbf{a}_2$, and $\mathbf{a}_3$ (Figure 3b). Once one of these two solutions for $\mathbf{b}_1$ is chosen, $\mathbf{a}_4$, $\mathbf{a}_5$, $\mathbf{b}_1$ and $\mathbf{b}_2$ define another tetrahedron with known edge lengths. Again, there are two possible mirror locations for $\mathbf{b}_2$, in this case with respect to the plane defined by $\mathbf{a}_4$, $\mathbf{a}_5$, and $\mathbf{b}_1$ (Figure 3c). Finally, after choosing one of the two solutions, $\mathbf{a}_6$, $\mathbf{b}_1$, $\mathbf{b}_2$, and $\mathbf{b}_3$ define another tetrahedron with known edge lengths. In this case there are two mirror possible locations for $\mathbf{b}_3$ with respect to the plane defined by $\mathbf{a}_6$, $\mathbf{b}_1$ and $\mathbf{b}_2$ (Figure 3d).

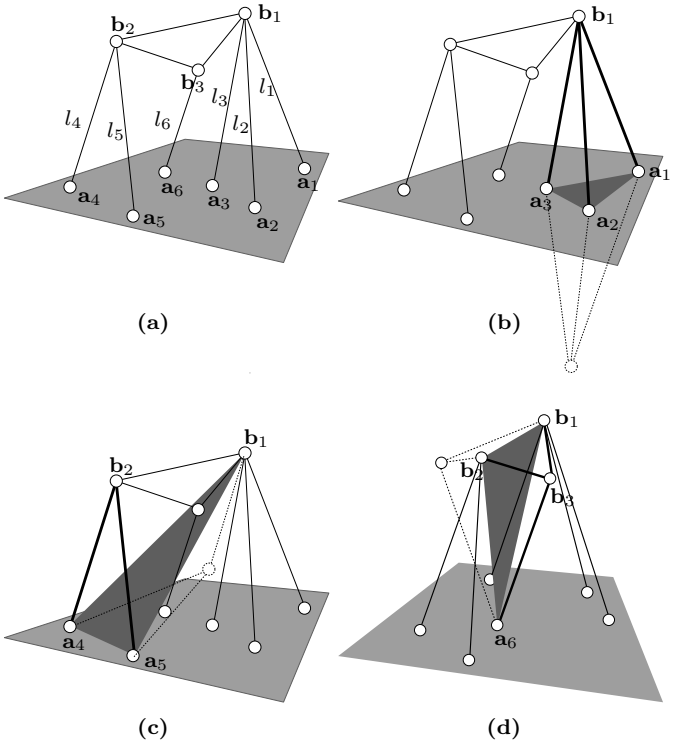

Fig. 3. General kinematic model of a 3-2-1 tracking system **(a)**. There are up to 8 possible solutions for the configuration of the platform compatible with a set of wire lengths due to the two possible solutions for the location of $\mathbf{b}_1$ **(b)**, $\mathbf{b}_2$ **(c)**, and $\mathbf{b}_3$ **(d)**.

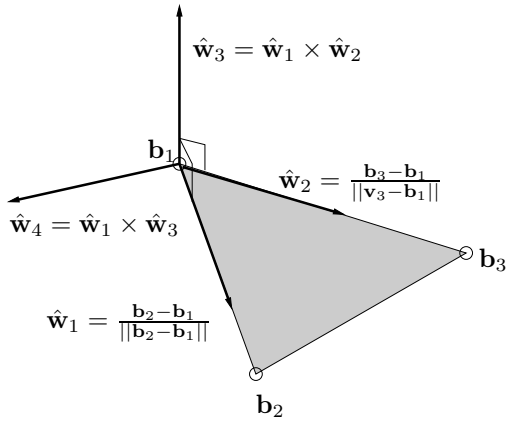

Fig. 4. Reference frame $(\hat{\mathbf{w}}_1, \hat{\mathbf{w}}_3, \hat{\mathbf{w}}_4)$ associated with the moving platform.

Once points $\mathbf{b}_1$, $\mathbf{b}_2$, and $\mathbf{b}_3$ have been located, they can be used to define a reference frame on the moving object. For example, according to Figure 4, the x-axis can be defined by the direction given by $\hat{\mathbf{w}}_1$, the y-axis can be chosen orthogonal to the plane defined by $\hat{\mathbf{w}}_1$ and $\hat{\mathbf{w}}_2$, and the z-axis can be obtained to give a Cartesian reference frame. These vectors form a set of orthogonal basis vectors whose directions are known relative to both the fixed and the moving reference frames. Note that this completely solves the forward kinematics of the 3-2-1 configuration without evaluating any trigonometric function.

There are certain singular sets of wire lengths in which

the number of solutions, for at least one of the three trilateration operations, is not two. For example, according to Equation (1), the first trilateration will yield only one solution if, and only if, $D(\mathbf{a}_1, \mathbf{a}_2, \mathbf{a}_3, \mathbf{b}_1) = 0$, i.e., if $\mathbf{a}_1$, $\mathbf{a}_2$, $\mathbf{a}_3$, and $\mathbf{b}_1$ lie on the same plane. Also, the result is undefined if, and only if, $D(\mathbf{a}_1, \mathbf{a}_2, \mathbf{a}_3) = 0$, i.e., if $\mathbf{a}_1$, $\mathbf{a}_2$, and $\mathbf{a}_3$ are aligned. Since $D(\mathbf{a}_1, \mathbf{a}_2, \mathbf{a}_3) = 0$ implies $D(\mathbf{a}_1, \mathbf{a}_2, \mathbf{a}_3, \mathbf{b}_1) = 0$, this latter condition encompasses all singularities for the first trilateration. This reasoning can be repeated for the other two trilaterations concluding that, if the platform is in a configuration in which

$$\begin{aligned} &D(\mathbf{a}_1, \mathbf{a}_2, \mathbf{a}_3, \mathbf{b}_1) = 0, \\ &D(\mathbf{a}_4, \mathbf{a}_5, \mathbf{b}_1, \mathbf{b}_2) = 0, \text{ or} \\ &D(\mathbf{a}_6, \mathbf{b}_1, \mathbf{b}_2, \mathbf{b}_3) = 0, \end{aligned} \tag{6}$$

the tracking system is in a singularity. In other words, these three determinants fully characterize all the singularities and, hence, a compact condition to test whether the system is in a singularity or not is given by

$$D(\mathbf{a}_1, \mathbf{a}_2, \mathbf{a}_3, \mathbf{b}_1) D(\mathbf{a}_4, \mathbf{a}_5, \mathbf{b}_1, \mathbf{b}_2) D(\mathbf{a}_6, \mathbf{b}_1, \mathbf{b}_2, \mathbf{b}_3) = 0, \tag{7}$$

which will be useful later.

Each equation in (6) implicitly defines an algebraic variety of dimension 5 that divides the configuration space of the platform, $\Re^3 \times SO(3)$, into two half-spaces. Then, the three equations in (6) lead to a partition of this configuration space into 8 regions. During normal operation, the tracking system should work in one of these regions without getting out of it to avoid ambiguities. Unfortunately, this is not the only reason to avoid a singularity. Near a singularity, small errors in the wire lengths induce important errors in the pose estimations not only in terms of their variances (this is discussed in Section IV) and also in their biases (this is discussed in Section V).

IV. Sensitivity to wire length errors

In what follows we will assume that the measured wire lengths are corrupted by random noise with gaussian probability density function and we will show how this error contributes to the measured pose error.

Let $\mathbf{l} = (l_1 \ l_2 \ \dots \ l_6)^t$ be the vector of measured wire lengths. Also, let $\mathbf{l}^0 = (l_1^0 \ l_2^0 \ \dots \ l_6^0)^t$ and $\delta\mathbf{l} = (\delta l_1 \ \delta l_2 \ \dots \ \delta l_6)^t$ be the vectors of the wire length actual values and the corresponding additive random errors, respectively. Then, $\mathbf{l} = \mathbf{l}^0 + \delta\mathbf{l}$. The wire length errors are assumed to have zero mean value, that is

$$E\{\delta\mathbf{l}\} = 0, \tag{8}$$

where $E\{\cdot\}$ stands for the expected value operation. We also assume that the wire length errors are uncorrelated with the same variance σ_r^2. Consequently their covariance matrix can be expressed as

$$E\{\delta\mathbf{l} \ \delta\mathbf{l}^t\} = \sigma_r^2 \mathbf{I}, \tag{9}$$

where $\mathbf{I}$ denotes the identity matrix.

Let $\mathbf{q} \in \Re^3 \times SO(3)$ be the platform configuration vector and $\mathbf{J}$ the mapping from the platform twist vector, $\dot{\mathbf{q}}$, to the wire length velocities, $\dot{\mathbf{l}}$, that is, $\dot{\mathbf{l}} = \mathbf{J}\dot{\mathbf{q}}$. Then,

$$\delta\mathbf{l} = \mathbf{l} - \mathbf{l}^0 \simeq \mathbf{J}(\mathbf{q} - \mathbf{q}^0) = \mathbf{J}\delta\mathbf{q} \tag{10}$$

Hence,

$$E\{\delta\mathbf{l} \ \delta\mathbf{l}^t\} = \mathbf{J} E\{\delta\mathbf{q} \ \delta\mathbf{q}^t\} \mathbf{J}^t = \sigma_r^2 \mathbf{I}. \tag{11}$$

Finally, the covariance matrix for the pose is

$$E\{\delta\mathbf{q} \ \delta\mathbf{q}^t\} = \sigma_r^2 \mathbf{J}^{-1} (\mathbf{J}^t)^{-1} = \sigma_r^2 (\mathbf{J}^t \mathbf{J})^{-1}. \tag{12}$$

Note that (12) is well-defined provided that $\mathbf{J}$ is nonsingular. It can be checked that the rows of $\mathbf{J}$ are the Plücker coordinates of lines (see, for example, [13]). Then, it is possible to characterize the singularities of $\mathbf{J}$, i.e. configurations in which $\det(\mathbf{J}) = 0$, in terms of the geometry of linearly dependent sets of lines. The set of conditions is typical for many parallel manipulators [18]. Nevertheless, in our case, according to the results presented in [7] for the 3-2-1 configuration, we know that

$$\det(\mathbf{J}) = 216 \frac{V_1 V_2 V_3}{l_1 l_2 l_3 l_4 l_5 l_6}, \tag{13}$$

where V_1, V_2, and V_3 are the volumes of the tetrahedra $\mathbf{a}_1\mathbf{a}_2\mathbf{a}_3\mathbf{b}_1$, $\mathbf{a}_4\mathbf{a}_5\mathbf{b}_2\mathbf{b}_3$, and $\mathbf{a}_6\mathbf{b}_1\mathbf{b}_2\mathbf{b}_3$, respectively. Then, using Equation (3), we conclude that

$$\det(\mathbf{J}) = \frac{\sqrt{D(\mathbf{a}_1, \mathbf{a}_2, \mathbf{a}_3, \mathbf{b}_1) D(\mathbf{a}_4, \mathbf{a}_5, \mathbf{b}_2, \mathbf{b}_3) D(\mathbf{a}_6, \mathbf{b}_1, \mathbf{b}_2, \mathbf{b}_3)}}{l_1 l_2 l_3 l_4 l_5 l_6}, \tag{14}$$

which fully agrees with the characterization of the singularities given by Equation (7), obtained using pure geometric arguments.

One of the key issues of any wire-based tracking device is its sensitivity to wire length errors. Since the actual configuration of the platform is contained in the ellipsoid

$$\{\mathbf{q} \in \Re^3 \times SO(3) \mid (\mathbf{q} - \mathbf{q}^0)^t \mathbf{J}^t \mathbf{J} (\mathbf{q} - \mathbf{q}^0) \leq 16\sigma_r^2\} \tag{15}$$

with probability 0.99 [21], it might seem reasonable to use the volume of this ellipsoid, that is,

$$\frac{1/6\pi^3}{\sqrt{\det\left(\frac{\mathbf{J}^t\mathbf{J}}{16\sigma_r^2}\right)}} \simeq \frac{63488}{3} \cdot \frac{\sigma_r^6}{\det(\mathbf{J})}, \tag{16}$$

as the measurement of this sensitivity. Then, using (14) and (16), and removing all constant factors, it seems reasonable to use

$$\mathcal{S} = \frac{l_1 l_2 l_3 l_4 l_5 l_6}{\sqrt{D(\mathbf{a}_1, \mathbf{a}_2, \mathbf{a}_3, \mathbf{b}_1) D(\mathbf{a}_4, \mathbf{a}_5, \mathbf{b}_2, \mathbf{b}_3) D(\mathbf{a}_6, \mathbf{b}_1, \mathbf{b}_2, \mathbf{b}_3)}} \tag{17}$$

as a sensitivity index of the 3-2-1 configuration to wire length errors. Note that this index is independent from the chosen reference frames and, what is more important, it can be interpreted either as the volume of the uncertainty ellipsoid in the configuration space of the platform, or as the reciprocal of the product of three tetrahedra volumes in the working space.

V. Bias error

Although the noise in the length measurements is assumed to have zero mean value, we show in this section that the expected value of the estimation error obtained by trilateration does not equal zero due to nonlinearities. Moreover, this kind of error –technically known as bias error– is only attributable to wire length errors. We also show in this section that zero mean gaussian errors in the base points do not contribute to any bias.

We only analyze the bias error for a single trilateration keeping in mind that, in a 3-2-1 configuration, its effect is carried forward along the three consecutive trilaterations.

A. Bias due to base point location errors

Following the notation in Figure 2, let $\delta\mathbf{p}_i$ and $\mathbf{p}_i^0$ denote the additive random error and the actual location of $\mathbf{p}_i$, $i = 1, 2, 3$, respectively. Then, $\mathbf{p}_i = \mathbf{p}_i^0 + \delta\mathbf{p}_i$. These errors are assumed to have zero mean value, that is $E\{\delta\mathbf{p}_i\} = 0$. We also assume that the errors in their three coordinates are uncorrelated with the same variance σ_s^2. In other words,

$$E\{\delta\mathbf{p}_i\ \delta\mathbf{p}_j^t\} = \begin{cases} \sigma_s^2\mathbf{I}, & \text{if } i = j \\ E\{\delta\mathbf{p}_i\}E\{\delta\mathbf{p}_j^t\} = \mathbf{0}, & \text{if } i \neq j \end{cases} \quad (18)$$

Remind that, if two gaussian random variables, say $\mathbf{a}$ and $\mathbf{b}$, are uncorrelated, they are independent [21], that is, $E(\mathbf{ab}) = E(\mathbf{a})E(\mathbf{b})$. Then, using (1), it is easy to check that

$$\begin{aligned}\delta\mathbf{p}_4 = \mathbf{p}_4 - \mathbf{p}_4^0 = \delta\mathbf{p}_1 + k_1\delta\mathbf{v}_1 + k_2\delta\mathbf{v}_2 \\ \pm k_3\left[(\mathbf{v}_1^0 \times \delta\mathbf{v}_2) + (\delta\mathbf{v}_1 \times \mathbf{v}_2^0) + (\delta\mathbf{v}_1 \times \delta\mathbf{v}_2)\right]\end{aligned} \quad (19)$$

where $\delta\mathbf{v}_1 = \delta\mathbf{p}_2 - \delta\mathbf{p}_1$ and $\delta\mathbf{v}_2 = \delta\mathbf{p}_3 - \delta\mathbf{p}_1$. Then, the bias error due to the error in the location of the base points can be obtained as follows:

$$\begin{aligned}E\{\delta\mathbf{p}_4\} &= \pm k_3 E\{\delta\mathbf{v}_1 \times \delta\mathbf{v}_2\} \\ &= \pm k_3 E\{(\delta\mathbf{p}_1 \times \delta\mathbf{p}_2) + (\delta\mathbf{p}_2 \times \delta\mathbf{p}_3) + (\delta\mathbf{p}_3 \times \delta\mathbf{p}_1)\},\end{aligned}$$

which is identically zero because all scalar products required to compute the above cross products involve uncorrelated random variables.

B. Bias due to length errors

Following the analysis for the single trilateration operation shown in Figure 2, the error in the location of $\mathbf{p}_4$, due to small wire length errors, can be well approximated by retaining the terms up to the second-order partial derivatives in the Taylor expansion of Equation (1), that is

$$\delta\mathbf{p}_4 = \mathbf{p}_4 - \mathbf{p}_4^0 = \sum_{i=1}^{3} \frac{\partial\mathbf{p}_4}{\partial l_i}\delta l_i + \frac{1}{2}\sum_{i=1}^{3}\sum_{j=1}^{3} \frac{\partial^2\mathbf{p}_4}{\partial l_i \partial l_j}\delta l_i \delta l_j. \quad (20)$$

The expected value of the random error in $\mathbf{p}_4$, i.e. the bias error, is

$$E\{\delta\mathbf{p}_4\} = \frac{1}{2}\sum_{i=1}^{3}\sum_{j=1}^{3} \frac{\partial^2\mathbf{b}_1}{\partial l_i \partial l_j} E\{\delta l_i\ \delta l_j\}. \quad (21)$$

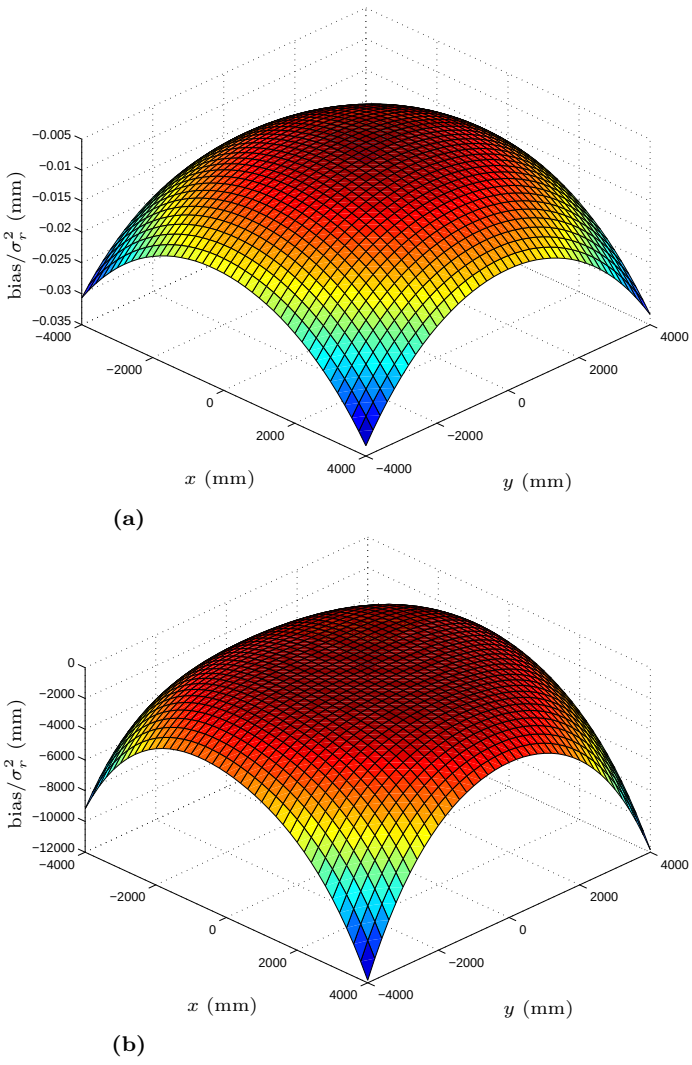

Fig. 5. For a representative example, component of the trilateration bias error orthogonal to the base plane for a distance of 4000 **(a)**, and 40 millimeters **(b)**.

Then, using (9),

$$E\{\delta\mathbf{p}_4\} = \frac{\sigma_r^2}{2}\left(\frac{\partial^2\mathbf{p}_4}{\partial l_1^2} + \frac{\partial^2\mathbf{p}_4}{\partial l_2^2} + \frac{\partial^2\mathbf{p}_4}{\partial l_3^2}\right). \quad (22)$$

Finally, substituting (1),

$$E\{\delta\mathbf{p}_4\} = \frac{\sigma_r^2}{2}(\nabla^2 k_1\mathbf{v}_1 + \nabla^2 k_2\mathbf{v}_2 \pm \nabla^2 k_3(\mathbf{v}_1 \times \mathbf{v}_2)), \quad (23)$$

where $\nabla^2 k_i = \frac{\partial^2 k_i}{\partial l_1^2} + \frac{\partial^2 k_i}{\partial l_2^2} + \frac{\partial^2 k_i}{\partial l_3^2}$ and the $+$ or $-$ sign is used depending on the chosen trilateration solution. The analytic expression for these derivatives can be found in Appendix I.

It is important to realize that the terms multiplying $\mathbf{v}_1$ and $\mathbf{v}_2$ are constant, i.e the bias error parallel to the base plane is constant, independently of the location of $\mathbf{p}_4$.

The trilateration bias error was already examined in [15], in the context of aeronautic navigation, where two main results were drawn:

(R1) The projection of the bias error onto the base plane can be neglected.
(R2) The bias error becomes relevant as $\mathbf{p}_4$ approaches the base plane.

Contrarily to all other formulations, these two facts have a direct accommodation in ours. As a consequence of (R1), Equation (23) can be approximated by

$$E\{\delta\mathbf{p}_4\} \simeq \pm\frac{\sigma_r^2}{2}\nabla^2 k_3(\mathbf{v}_1 \times \mathbf{v}_2), \tag{24}$$

and, as a consequence of (R2), this equation can be further simplified, near a singularity, into

$$E\{\delta\mathbf{p}_4\} \simeq \mp\sigma_r^2\frac{l_1^2A_3^2 + l_2^2A_2^2 + l_3^2A_1^2}{54V^3}(\mathbf{v}_1 \times \mathbf{v}_2), \tag{25}$$

where A_1, A_2, and A_3 are the areas of the triangles $\mathbf{p}_r\mathbf{p}_2\mathbf{p}_3$, $\mathbf{p}_r\mathbf{p}_1\mathbf{p}_3$, and $\mathbf{p}_r\mathbf{p}_1\mathbf{p}_2$, respectively, $\mathbf{p}_r$ being the orthogonal projection of $\mathbf{p}_4$ onto the plane defined by $\mathbf{p}_1$, $\mathbf{p}_2$ and $\mathbf{p}_3$, and V is the volume of the tetrahedron $\mathbf{p}_1\mathbf{p}_2\mathbf{p}_3\mathbf{p}_4$ (see Appendix I for the details). Equation (25) is remarkable because its simplicity (compare it to the result presented in [15]).

It can be checked that, as a consequence of this error, when $\mathbf{p}_4$ moves on a plane parallel to that of the three base points, the estimation will erroneously indicate that it ascends and descends when it approaches to, and goes away from the barycenter of the base points, respectively. Note that, since this is a systematic error, it can be compensated by proper calibration.

Figure 5 examines this error for a representative case. Consider that the three base points form an equilateral triangle on the XY plane inscribed in a circle centered in the origin of radius 1000 millimeters. The base points are $\mathbf{p}_1 = (500\sqrt{3}, -500, 0)^t$, $\mathbf{p}_2 = (0, 1000, 0)^t$, and $\mathbf{p}_3 = (-500\sqrt{3}, -500, 0)^t$. The data acquisition area of the system is an XY plane square area, at a distance of 4000 millimeters of the base plane, spanning in each direction from -4000 to 4000 millimeters. The maximum bias error in this region is $-0.03\sigma_r^2$ millimeters (Figure 5a), which can be neglected in practice. This amount exponentially increases as $\mathbf{p}_4$ reduces its distance to the base plane, i.e. the singularity is approached. When the distance is 400 millimeters, the maximum bias error is $-12\sigma_r^2$, and when it is reduced to 40 millimeters the maximum bias error mounts to $-11842\sigma_r^2$ (Figure 5b).

We conclude that near a singularity not only random errors are amplified but also estimations are highly biased. As exemplified in the next section, the destructive combination of both effects makes any practical measurement near a singularity almost useless.

VI. Experimental results

The validation of the obtained theoretical results has been carried out by tracking the motion of the end effector of a PUMA 562 robot, both using a real system [20], and a simulation tool [23] (Figure 6). The simulations has been proved of great interest to compare the estimations obtained from noisy experimental data to those obtained without noise near singularities in simulation.

$\mathbf{a}_1$	(500, 500, -1000)
$\mathbf{a}_2$	(250, 933, -1000)
$\mathbf{a}_3$	(-250, 933, -1000)
$\mathbf{a}_4$	(-500, 500, -1000)
$\mathbf{a}_5$	(-250, 67, -1000)
$\mathbf{a}_6$	(250, 67, -1000)

$\mathbf{b}_1$	(-100,0,50)
$\mathbf{b}_2$	(100,0,50)
$\mathbf{b}_3$	(0,100,50)

TABLE I
Coordinates (in millimeters) of the base and platform articulation centers referred to the reference frames shown in Figure 6b and c, respectively.

The implemented mechatronic system was conceived at the Laboratory of Robotics and Mechatronics in Cassino where a prototype is currently in use for robot workspace evaluation [4]. It consists of a mechanical part and an interface connected to a personal computer. The signals from the wire transducers, which have a working range of $1.5m$, are feeded through an amplifier to a 12 bits A/D board installed on the computer. The articulation centers on the base have been arranged forming an hexagon. Their coordinates, as well as those of the platform attachments, can be found in Table I. These coordinates are referenced to the frames shown in Figure 6b and c, respectively.

Due to physical limitations, the implemented wire-based device only works in one of the two half-spaces defined by the base plane. Since the result of the first trilateration should be taken in the right half-space, the number of forward kinematic solutions is reduced to four. Note that these four solutions always come in two couples sharing the same sensitivity index because the corresponding volumes of the tetrahedra involved in the second and third trilaterations are the same for them.

A. First experiment

This experiment consists in approaching the robot end-effector to the base plane moving only the second articulation of the robot so that the x coordinates of the attachments in the platform are kept constant at 250 millimeters. Figure 7a shows how the six wire lengths evolve along this trajectory. Figure 7b, c, and d show the coordinates of $\mathbf{b}_3$ compatible with these lengths obtained as the result of the three consecutive trilaterations, thus accumulating all possible errors. The plots in thick line correspond to the actual motion executed by $\mathbf{b}_3$.

The interesting point about this experiment is that two of the four possible solution branches cross at a singularity (actually, a singularity can also be seen as a configuration in which two solution branches intersect). Note the great noise amplification near the singularity for these two crossing branches, while the other two remain stable, and how this noise makes that at some points no solution exists for a trilateration, leading to a discontinuity. This gives rise to an important question: when there is no solution for

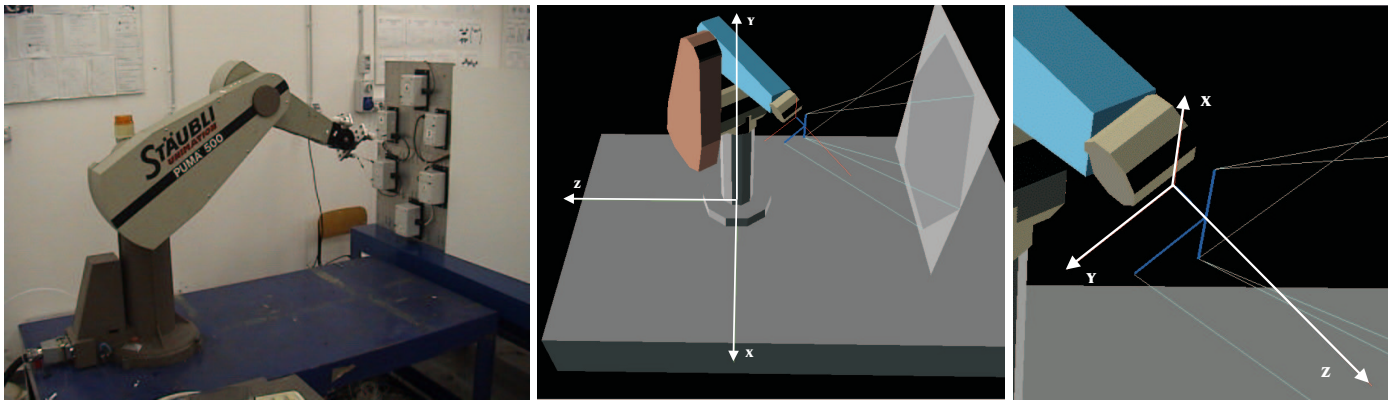

(a) **(b)** **(c)**

Fig. 6. Experimental setup **(a)**, and graphics simulation of the tracking device connected to a PUMA robot **(b)**, **(c)**.

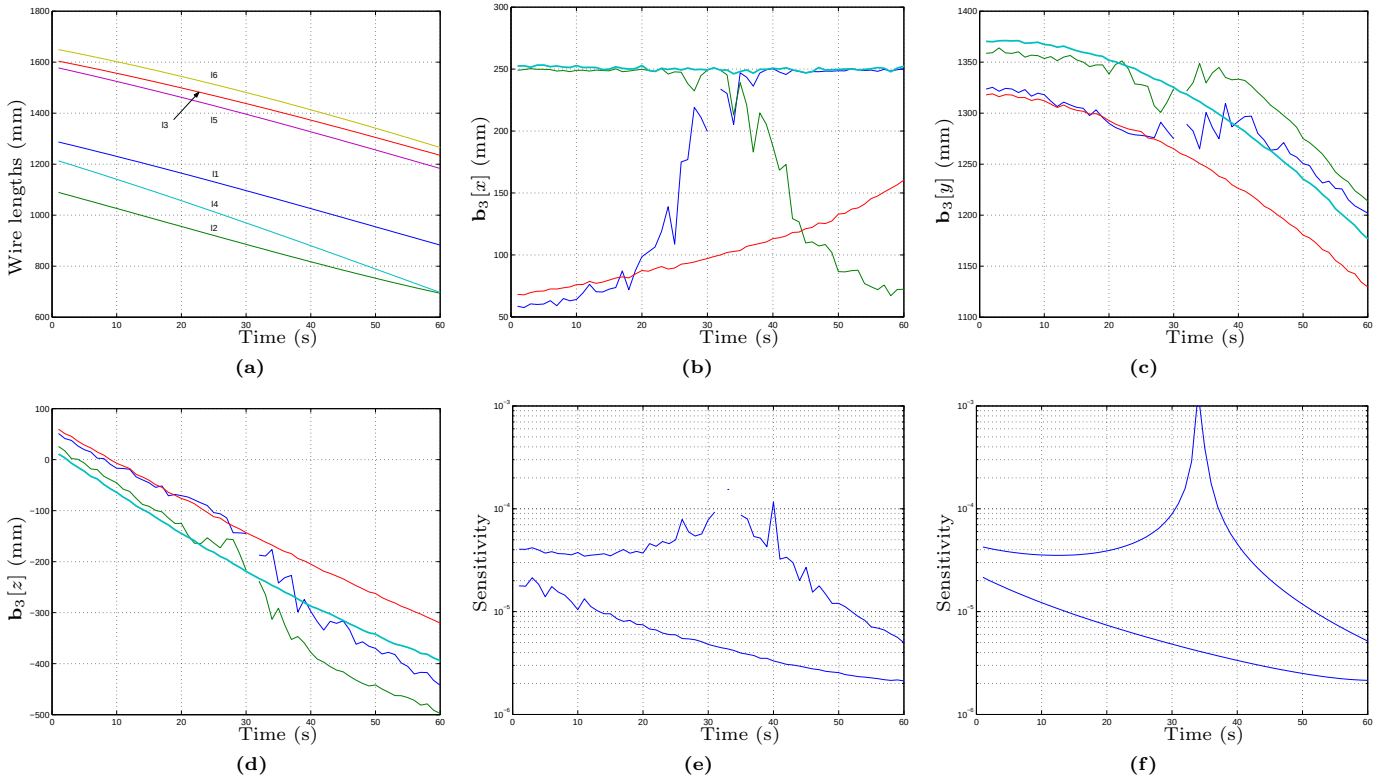

(a) **(b)** **(c)**

(d) **(e)** **(f)**

Fig. 7. First experiment. Two solution branches crossing at a singularity.

a trilateration operation due to errors, which is the best estimation for the solution? An easy way to generate an approximate solution is to argue that, because the negative value of the determinant inside the square root in the trilateration formulation outlined in Section II is due to errors in the lengths, it is reasonable so set this square root to zero. Unfortunately, this simple device does not always provide an acceptable approximation and, as it was shown in [5], one has to solve in general a nonlinear least square problem.

Figure 7e and f show the sensitivity index defined in Equation (17) obtained from experimental and noiseless simulated data, respectively. Note that, while the two stable solutions keep a low sensitivity, that for the crossing solutions goes to infinity at the singularity. This means that the uncertainty ellipsoid in the configuration space of the platform becomes unbounded and at least one of the three tetrahedra involved in the trilaterations becomes planar.

At the beginning of a measuring cycle, the pose of the platform can be assumed to be known. This would require deciding the orientation of the tetrahedron involved in the second and third trilateration which could be done by visual inspection, or adding extra sensors such as inclinometers. If a singularity is traversed, an ambiguity arises because two solution branches cross. In theory, since infinity

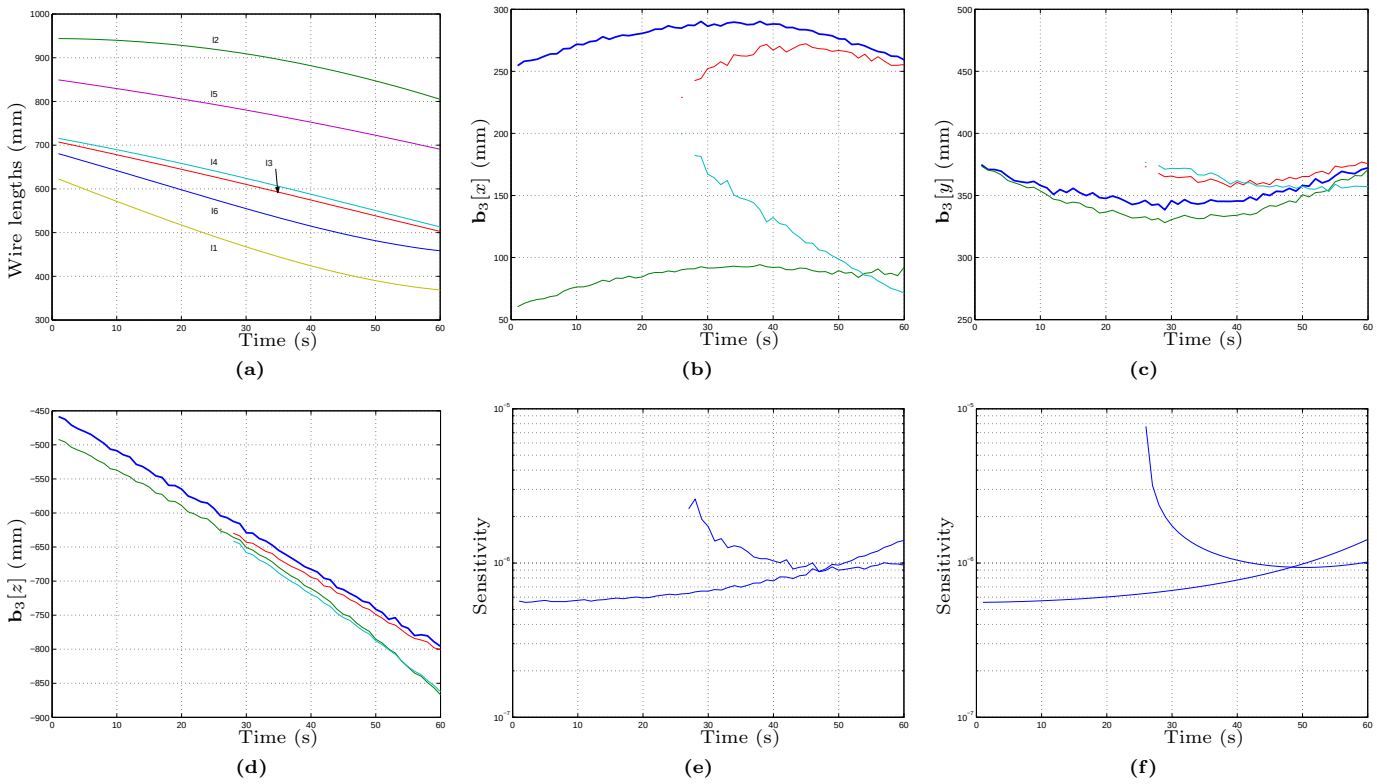

Fig. 8. Second experiment. Two solution branches vanishing at a singularity.

accelerations are not physically feasible, it seems reasonable to design an algorithm able to track a unique solution based on the continuity of the velocity vector. Unfortunately, in practice, due to the noise amplification near a singularity, as this experiment has exemplified, this possibility seems unfeasible.

B. Second experiment

This experiment consists in approaching the robot end-effector to the base plane using a joint interpolated motion. Figure 8a shows how the six wire lengths evolve along this trajectory. Figure 8b, c, and d show the coordinates of $\mathbf{b}_3$ compatible with these lengths obtained as the result of the three consecutive trilaterations. The plots in thick line correspond to the actual motion executed by $\mathbf{b}_3$.

The interesting point about this experiment is that at the beginning of the trajectory only two solutions are possible. At $t = 28$ two other solutions arise to complete the set of four possible solutions. A closer analysis reveals that these two new solutions emerge from a singularity. As in the previous example, the exact point where the two solution branches met cannot be properly observed because, due to error amplification near a singularity, no solution to some trilaterations can be found. Obviously, solution branches that meet and vanish at a singularity do not correspond to real solutions. Thus, although in theory up to four solutions are possible, two could be rejected on this basis.

Figures 8e and f show the sensitivity index obtained from experimental and noiseless simulated data, respectively. Note how the proposed sensitivity index is of practical interest as it provides a quality measurement of the obtained estimations directly from experimental data.

C. Third experiment

There is no bias without noise. Then, the problem of exemplifying bias errors is that they are significant near singularities, precisely where noise is highly amplified, as it has been shown in the previous experiments. Since errors are assumed to have zero mean value, in this experiment we will try to distinguish bias from noise by averaging the result of multiple realizations of the same experiment.

This third experiment consists in moving the robot end-effector so that the y and z coordinates of the platform attachments vary within a narrow range of 1mm along a trajectory of 400mm. This permits expanding the scale for these two coordinates to analyze the effect of bias errors in detail. Figure 9a shows how the six wire lengths evolve along the chosen trajectory. Figure 9b, c, and d show the coordinates of $\mathbf{b}_1$ compatible with these lengths obtained as the result of the first trilateration.

The plots in thick line correspond to the actual motion executed by $\mathbf{b}_1$ obtained by simulation. The noisy plots correspond to the result of averaging 50 realizations of the same experiment. The results do not exhibit any apparent bias. This does not contradict the obtained theoretical results because the error in the wire lengths is quite low and the measurements have been taken next to the barycenter of the base points $\mathbf{a}_1$, $\mathbf{a}_2$, and $\mathbf{a}_3$ where the bias error is known to be minimum. Nevertheless, by adding gaussian

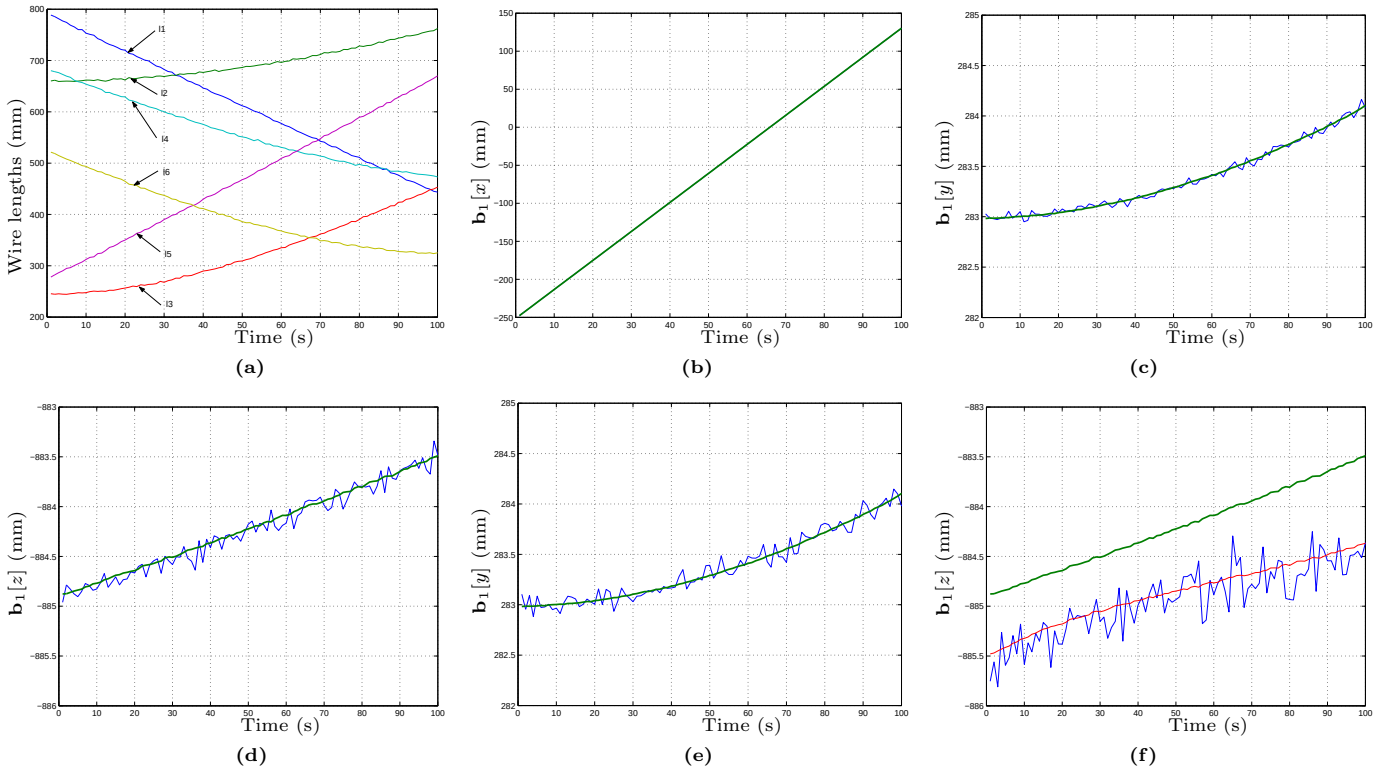

Fig. 9. Third experiment. The effect of bias errors.

noise to the length measurements with a variance of 5 millimeters and averaging the result of 500 realizations, the y coordinate is kept unbiased (Figure 9e) but a clear bias error arises in the z coordinate (Figure 9f), that is, in the component orthogonal to the base plane. This fully agrees with the theoretical results outlined in Section V. Also, in Figure 9e, the bias error obtained from Equation (25) with $\sigma_r = 5$mm has been added to the result obtained without noise and plotted in thin line. Since the final result is a good approximation of the averaged result with noise, it seems feasible to identify the variance of the wire length errors by analyzing the bias errors.

VII. Conclusions

A performance analysis of a 3-2-1 pose estimation device has been presented. It has been shown how, near a singularity, small errors in the wire lengths induce important errors in the pose estimations not only in terms of their variances and also in their biases.

Concerning the variances of the pose estimations, a sensibility index for the estimations have been proposed which has been proved of practical interest as it provides a quality measurement of the obtained estimations directly from experimental data.

Concerning the bias error, an asymptotic formula of remarkable simplicity for this error has been obtained thanks to a closed-form solution to the forward kinematics of the device in terms of Cayley-Menger determinants. It have been shown how all algebraic manipulations based on this formulation can be performed involving only distances, and the results can always been interpreted in terms of lengths, areas and volumes. This has been revealed of great interest when calculating the required partial derivatives with respect to wire lengths to obtain the aforementioned asymptotic formula. It is also worth highlighting here that bias errors have been omitted in previous analysis of wire-based tracking devices.

The device has been analyzed for static pose estimations but, in general, this device has interest for estimating trajectories, that is for tracking purposes. The measurements along a trajectory are not statistically uncorrelated so that they should be jointly smoothed during tracking to improve accuracy using, for example, a Kalman filter. The performance analysis given in this paper is of relevance to this end. For example, the characterization of the bias error must not be ignored at this point and it has to be suitably anticipated in this filter. This issue deserves further research.

Appendix

This appendix is devoted to compute second derivatives of k_1, k_2 and k_3 with respect to l_1, l_2 and l_3. To start, note that, since the denominator in

$$k_1 = -\frac{D(\mathbf{p}_1, \mathbf{p}_2, \mathbf{p}_3; \mathbf{p}_1, \mathbf{p}_3, \mathbf{p}_4)}{D(\mathbf{p}_1, \mathbf{p}_2, \mathbf{p}_3)}$$

does not depend on l_1, l_2 or l_3, then

$$\frac{\partial^2 k_1}{\partial l_j^2} = \frac{-1}{D(\mathbf{p}_1, \mathbf{p}_2, \mathbf{p}_3)} \cdot \frac{\partial^2 D(\mathbf{p}_1, \mathbf{p}_2, \mathbf{p}_3; \mathbf{p}_1, \mathbf{p}_3, \mathbf{p}_4)}{\partial {l_j}^2}$$

and we only need the second derivatives of

$$D(\mathbf{p}_1,\mathbf{p}_2,\mathbf{p}_3;\mathbf{p}_1,\mathbf{p}_3,\mathbf{p}_4) = -\frac{1}{4}\begin{vmatrix} 0 & 1 & 1 & 1 \\ 1 & 0 & D(\mathbf{p}_1,\mathbf{p}_3) & l_1^2 \\ 1 & D(\mathbf{p}_1,\mathbf{p}_2) & D(\mathbf{p}_2,\mathbf{p}_3) & l_2^2 \\ 1 & D(\mathbf{p}_1,\mathbf{p}_3) & 0 & l_3^2 \end{vmatrix}$$

with respect to l_1, l_2 and l_3. By expanding this determinant by the last column, we easily realize that

$$\begin{aligned} \frac{\partial D(\mathbf{p}_1,\mathbf{p}_2,\mathbf{p}_3;\mathbf{p}_1,\mathbf{p}_3,\mathbf{p}_4)}{\partial l_1} &= -D(\mathbf{p}_2,\mathbf{p}_3;\mathbf{p}_1,\mathbf{p}_3)\, l_1, \\ \frac{\partial D(\mathbf{p}_1,\mathbf{p}_2,\mathbf{p}_3;\mathbf{p}_1,\mathbf{p}_3,\mathbf{p}_4)}{\partial l_2} &= D(\mathbf{p}_1,\mathbf{p}_3)\, l_2, \\ \frac{\partial D(\mathbf{p}_1,\mathbf{p}_2,\mathbf{p}_3;\mathbf{p}_1,\mathbf{p}_3,\mathbf{p}_4)}{\partial l_3} &= -D(\mathbf{p}_1,\mathbf{p}_2;\mathbf{p}_1,\mathbf{p}_3)\, l_3, \end{aligned}$$

and, hence, that

$$\begin{aligned} \frac{\partial^2 k_1}{\partial l_1^2} &= \frac{D(\mathbf{p}_2,\mathbf{p}_3;\mathbf{p}_1,\mathbf{p}_3)}{D(\mathbf{p}_1,\mathbf{p}_2,\mathbf{p}_3)}, \\ \frac{\partial^2 k_1}{\partial l_2^2} &= -\frac{D(\mathbf{p}_1,\mathbf{p}_3)}{D(\mathbf{p}_1,\mathbf{p}_2,\mathbf{p}_3)}, \\ \frac{\partial^2 k_1}{\partial l_3^2} &= \frac{D(\mathbf{p}_1,\mathbf{p}_2;\mathbf{p}_1,\mathbf{p}_3)}{D(\mathbf{p}_1,\mathbf{p}_2,\mathbf{p}_3)}. \end{aligned}$$

Then, after substituting the above determinants by their geometric interpretations,

$$\nabla^2 k_1 = \frac{b^2}{8A_b^2}, \tag{26}$$

where A_b is the area of the triangle $\mathbf{p}_1\mathbf{p}_2\mathbf{p}_3$ and b the length of the edge $\mathbf{p}_1\mathbf{p}_3$.

Proceeding in an analogous way for k_2 we obtain:

$$\begin{aligned} \frac{\partial^2 k_2}{\partial l_1^2} &= -\frac{D(\mathbf{p}_2,\mathbf{p}_3;\mathbf{p}_1,\mathbf{p}_2)}{D(\mathbf{p}_1,\mathbf{p}_2,\mathbf{p}_3)}, \\ \frac{\partial^2 k_2}{\partial l_2^2} &= \frac{D(\mathbf{p}_1,\mathbf{p}_3;\mathbf{p}_1,\mathbf{p}_2)}{D(\mathbf{p}_1,\mathbf{p}_2,\mathbf{p}_3)}, \\ \frac{\partial^2 k_2}{\partial l_3^2} &= -\frac{D(\mathbf{p}_1,\mathbf{p}_2)}{D(\mathbf{p}_1,\mathbf{p}_2,\mathbf{p}_3)}. \end{aligned}$$

Then,

$$\nabla^2 k_2 = \frac{a^2}{8A_b^2}, \tag{27}$$

where a the length of the edge $\mathbf{p}_1\mathbf{p}_2$.

With regard to the second derivatives of k_3 it can easily be checked that, by applying the chain rule to

$$k_3 = \frac{\sqrt{D(\mathbf{p}_1,\mathbf{p}_2,\mathbf{p}_3,\mathbf{p}_4)}}{D(\mathbf{p}_1,\mathbf{p}_2,\mathbf{p}_3)},$$

we get

$$\frac{\partial^2 k_3}{\partial {l_j}^2} = \frac{1}{48A_b^2V}\eta - \frac{1}{3456A_b^2V^3}\mu^2. \tag{28}$$

where $\eta = \frac{\partial^2 D(\mathbf{p}_1,\mathbf{p}_2,\mathbf{p}_3,\mathbf{p}_4)}{\partial {l_j}^2}$, $\mu = \frac{\partial D(\mathbf{p}_1,\mathbf{p}_2,\mathbf{p}_3,\mathbf{p}_4)}{\partial l_j}$, and V is the volume of the tetrahedron $\mathbf{p}_1\mathbf{p}_2\mathbf{p}_3\mathbf{p}_4$. Then, it only remains to compute the first and second derivatives of $D(\mathbf{p}_1,\mathbf{p}_2,\mathbf{p}_3,\mathbf{p}_4)$ with respect to the desired length. To this end, we write

$$D(\mathbf{p}_1,\mathbf{p}_2,\mathbf{p}_3,\mathbf{p}_4) = \frac{1}{8}\begin{vmatrix} 0 & 1 & 1 & 1 & 1 \\ 1 & 0 & D(\mathbf{p}_1,\mathbf{p}_2) & D(\mathbf{p}_1,\mathbf{p}_3) & l_1^2 \\ 1 & D(\mathbf{p}_1,\mathbf{p}_2) & 0 & D(\mathbf{p}_2,\mathbf{p}_3) & l_2^2 \\ 1 & D(\mathbf{p}_1,\mathbf{p}_3) & D(\mathbf{p}_2,\mathbf{p}_3) & 0 & l_3^2 \\ 1 & l_1^2 & l_2^2 & l_3^2 & 0 \end{vmatrix},$$

and realize that

$$\begin{aligned} \tfrac{\partial D(\mathbf{p}_1,\mathbf{p}_2,\mathbf{p}_3,\mathbf{p}_4)}{\partial l_1} &= 2l_1 D(\mathbf{p}_1,\mathbf{p}_2,\mathbf{p}_3;\mathbf{p}_3,\mathbf{p}_2,\mathbf{p}_4), \\ \tfrac{\partial D(\mathbf{p}_1,\mathbf{p}_2,\mathbf{p}_3,\mathbf{p}_4)}{\partial l_2} &= 2l_2 D(\mathbf{p}_1,\mathbf{p}_2,\mathbf{p}_3;\mathbf{p}_1,\mathbf{p}_3,\mathbf{p}_4), \\ \tfrac{\partial D(\mathbf{p}_1,\mathbf{p}_2,\mathbf{p}_3,\mathbf{p}_4)}{\partial l_3} &= 2l_3 D(\mathbf{p}_1,\mathbf{p}_2,\mathbf{p}_3;\mathbf{p}_2,\mathbf{p}_1,\mathbf{p}_4). \end{aligned} \tag{29}$$

Then, proceeding as for k_1 and k_2, we get

$$\begin{aligned} \tfrac{\partial D^2(\mathbf{p}_1,\mathbf{p}_2,\mathbf{p}_3,\mathbf{p}_4)}{\partial l_1^2} &= 2D(\mathbf{p}_1,\mathbf{p}_2,\mathbf{p}_3;\mathbf{p}_3,\mathbf{p}_2,\mathbf{p}_4) + 2l_1^2c^2 \\ \tfrac{\partial D^2(\mathbf{p}_1,\mathbf{p}_2,\mathbf{p}_3,\mathbf{p}_4)}{\partial l_2^2} &= 2D(\mathbf{p}_1,\mathbf{p}_2,\mathbf{p}_3;\mathbf{p}_1,\mathbf{p}_3,\mathbf{p}_4) + 2l_2^2b^2 \\ \tfrac{\partial D^2(\mathbf{p}_1,\mathbf{p}_2,\mathbf{p}_3,\mathbf{p}_4)}{\partial l_3^2} &= 2D(\mathbf{p}_1,\mathbf{p}_2,\mathbf{p}_3;\mathbf{p}_2,\mathbf{p}_1,\mathbf{p}_4) + 2l_3^2a^2 \end{aligned} \tag{30}$$

Finally, after substituting Equations (29) and (30) into Equation (28), and expressing the result in terms of volumes, areas and lengths, we conclude that

$$\nabla^2 k_3 = \frac{1}{6V} + \frac{l_1^2c^2 + l_2^2b^2 + l_3^2c^2}{24A_b^2V} - \frac{l_1^2A_3^2 + l_2^2A_2^2 + l_3^2A_1^2}{54V^3}, \tag{31}$$

where A_1, A_2, and A_3 are the areas of the triangles $\mathbf{p}_r\mathbf{p}_2\mathbf{p}_3$, $\mathbf{p}_r\mathbf{p}_1\mathbf{p}_3$, and $\mathbf{p}_r\mathbf{p}_1\mathbf{p}_2$, respectively, $\mathbf{p}_r$ being the orthogonal projection of $\mathbf{p}_4$ onto the plane defined by $\mathbf{p}_1$, $\mathbf{p}_2$ and $\mathbf{p}_3$, and c the length of the edge $\mathbf{p}_2\mathbf{p}_3$.

We are in a singularity of the trilateration if, and only if, $V = 0$. Then, near a singularity, Equation (31) can be approximated by

$$\nabla^2 k_3 \simeq -\frac{l_1^2A_3^2 + l_2^2A_2^2 + l_3^2A_1^2}{54V^3}. \tag{32}$$

Acknowledgements

This work has been partially supported by the Italian-Spanish Bilateral CSIC-CNR Cooperation Program

References

[1] L.M. Blumenthal, *Theory and Applications of Distance Geometry,* Oxford University Press, 1953.

[2] H. Bruyninckx, "Forward kinematics for Hunt-Primrose parallel manipulators," *Mechanism and Machine Theory*, Vol. 34, pp. 657-664, 1999.

[3] A. Cayley, "A theorem in the Geometry of Position," *Cambridge Mathematical Journal*, Vol. II, pp. 267-271, 1841. (Also in *Collected Mathematical Papers of Arthur Cayley*, Cambridge University Press, 1963).

[4] M. Ceccarelli, E. Ottaviano, and M. Toti, "Experimental determination of robot workspace by means of CATRASYS (Cassino Tracking System)," *Proc. of the 13th CISM IFToMM Symposium on Theory and Practice of Robots and Manipulators*, pp. 85-92, 2000.

[5] I.D. Coope, "Reliable computation of the points of intersection of n spheres in $\Re^n$, *Australian and New Zealand Industrial and Applied Mathematics Journal*, Part C, Vol. 42, pp. 461-477, 2000.

[6] G.M. Crippen and T. Havel, *Distance Geometry and Molecular Conformation*, John Wiley and Sons Inc., New York, 1988.

[7] D.M. Downing, A.E. Samuel, and K.H. Hunt, "Identification of the special configurations of the octaedral manipulator using the pure condition," *The International Journal of Robotics Research*, Vol. 21, No. 2, pp. 147-160, 2002.

[8] D. Eberly, "Finding the intersection of three spheres," comp.graphics.algorithms newsgroup, 1996.

[9] Z. Geng and L.S. Haynes, "A 3-2-1 kinematic configuration of a Stewart platform and its application to six degree of freedom pose measurements," *Robotics and Computer-Integrated Manufacturing*, Vol. 11, No. 1, pp. 23-34, 1994.

[10] M. Griffis and J. Duffy, "A forward displacement analysis of a class of Steward platforms," *Journal of Robotic Systems*, Vol. 6, No. 6, pp. 703-720, 1989.

[11] K.H. Hunt and E.J.F. Primrose, "Assembly configurations of some in-parallel-actuated manipulators," *Mechanism and Machine Theory*, Vol. 28, No. 1, pp. 31-42, 1993.

[12] J.W. Jeong, S.H. Kim, and Y.K. Kwak, "Kinematics and workspace analysis of a parallel wire mechanism for measuring a robot pose," *Mechanism and Machine Theory*, Vol. 34, No. 6, pp. 825-841, 1999.

[13] O. Ma and J. Angeles, "Architecture singularities of platform manipulators," *Proc. of the 1991 IEEE Int. Conf. on Robotics and Automation,* pp. 1542-1557, 1991.

[14] A.L. Mackay, "Generalized Structural Geometry," *Acta Crystalographica*, Vol. A-30, pp. 440-447, 1974.

[15] D.E. Manolakis, "Efficient solution and performance analysis of 3-D position estimation by trilateration," *IEEE Trans. on Aerospace and Electronic Systems,* Vol. 32, No. 4, pp. 1239-1248, 1996.

[16] P. Nanua and K.J. Waldron, "Direct kinematics solution of a special parallel robot structure," *Proc. of the 8 Cism-Iftomm Symposium*, pp. 134-142, 1990.

[17] P. Nanua, K.J. Waldron, and V. Murthy, "Direct kinematic solution of a Steward platform," *IEEE Trans. on Robotics and Automation*, Vol. 6, No. 4, pp. 438-444, 1990.

[18] J.M. McCarthy, *Geometric Design of Linkages*, Springer-Verlag, New York, 2000.

[19] K. Menger, "New foundation for Euclidean geometry," *American Journal of Mathematics,* No. 53, pp. 721-745, 1931.

[20] E. Ottaviano, M. Ceccarelli, M. Totti, and C. Avila-Carrasco, "CATRASYS (Cassino Tracking System): A wire system for experimental evaluation of robot workspace," *Journal of Robotics and Mechatronics,* Vol. 14, No. 1, pp. 78-87, 2002.

[21] A. Papoulis, *Probability, Random Variables and Stochastic Processes*, McGraw-Hill, 3rd edition, 1991.

[22] V. Parenti-Castelli and C. Innocenti, "Direct displacement analysis for some classes of spatial parallel machanisms," *Proc. of the 8th CISM IFToMM Symposium on Theory and Practice of Robots and Manipulators*, pp. 126-133, 1990.

[23] F. Thomas and L. Basañez, "Interactive planning using graphical simulation for robot task programming," *Proc. of the 10th CISM IFToMM Symposium on Theory and Practice of Robots and Manipulators*, pp. 378-385, 1993.

[24] F. Thomas, E. Ottaviano, L. Ros, and M. Ceccarelli, "Coordinate-free formulation of a 3-2-1 wire-based tracking device using Cayley-Menger determinants," *Proc. of the 2003 IEEE Int. Conf. on Robotics and Automation*, to appear.